

bradscholars

Coformer Replacement as an Indicator for Thermodynamic Instability of Cocrystals: Competitive Transformation of Caffeine:Dicarboxylic Acid

Item Type	Article
Authors	Alsirawan, MHD Bashir;Vangala, Venu R.;Kendrick, John;Leusen, Frank J.J.;Paradkar, Anant R
Citation	Alsirawan MHDB, Vangala VR, Kendrick J et al (2016) Coformer Replacement as an Indicator for Thermodynamic Instability of Cocrystals: Competitive Transformation of Caffeine:Dicarboxylic Acid. Crystal Growth & Design. 16(6): 3072-3075.
DOI	https://doi.org/10.1021/acs.cgd.6b00458
Rights	© 2016 ACS. This document is the Accepted Manuscript version of a Published Work that appeared in final form in Crystal Growth & Design, copyright © American Chemical Society after peer review and technical editing by the publisher. To access the final edited and published work see http://dx.doi.org/10.1021/acs.cgd.6b00458
Download date	2026-04-12 14:10:32
Link to Item	https://bradscholars.brad.ac.uk/handle/10454/8401.2

The University of Bradford Institutional Repository

<http://bradscholars.brad.ac.uk>

This work is made available online in accordance with publisher policies. Please refer to the repository record for this item and our Policy Document available from the repository home page for further information.

To see the final version of this work please visit the publisher's website. Available access to the published online version may require a subscription.

Link to publisher's version: <http://dx.doi.org/10.1021/acs.cgd.6b00458>

Citation: Alsirawan MHD B, Vangala VR, Kendrick J, Leusen FJ and Paradkar A (2016) Coformer Replacement as an Indicator for Thermodynamic Instability of Cocrystals: Competitive Transformation of Caffeine:Dicarboxylic Acid. [Supporting information]. *Crystal growth & design*. 16 (6): 3072-3075.

Copyright statement: © 2016 ACS. This document is the Accepted Manuscript version of the Supporting Information of a Published Work that appeared in final form in *Crystal Growth & Design*, copyright © American Chemical Society after peer review and technical editing by the publisher. To access the final edited and published work see <http://dx.doi.org/10.1021/acs.cgd.6b00458>.

Coformer Replacement as an Indicator for
Thermodynamic Instability of Cocrystals:
Competitive Transformation of
Caffeine:Dicarboxylic Acid

*MHD. Bashir Alsirawan,[†] Venu R. Vangala,[†] John Kendrick,[‡] Frank J. J. Leusen,[‡] and Anant
Paradkar^{*†}*

[†]Centre for Pharmaceutical Engineering Science, University of Bradford, Richmond Rd,
Bradford, West Yorkshire, BD7 1DP, UK. Email: A.Paradkar1@bradford.ac.uk

[‡]School of Chemistry and Forensic Science, University of Bradford.

Supporting Information

Table of Contents

Experimental Section.....	2
1) Cocrystal Preparation:.....	2
2) Mixing Processes:.....	3
3) Thermogravimetric Analysis (TGA):.....	4
4) Powder X-ray Diffraction (PXRD):.....	4
5) Equilibrium solubility determinations:.....	4
6) High performance liquid chromatography (HPLC) analysis:.....	4
7) Density functional theory method:.....	5
8) Gibbs free energy change equation derivation:.....	5
Supporting Results:.....	7
9) Characterisation of prepared cocrystals by PXRD:.....	7
10) Aqueous processing reactions:.....	8
11) Mechanical processing reactions:.....	12
12) Thermal gravimetric analysis (TGA):.....	18
13) DFT Computational data:.....	23
14) pH measurements:.....	24
15) Gibbs free energy change results:.....	25
Supporting References:.....	26

Experimental Section

All materials and organic solvents were purchased from Sigma-Aldrich Company (UK), Ltd and were used as received.

1) Cocrystal Preparation:

Caffeine:Dicarboxylic acid CA:DA cocrystals (Table S1) were obtained by solution crystallization as described by Trask and Jones¹. Slight modifications to their methods were required to prepare bulk materials:

Caffeine:Oxalic acid, CA:OX: anhydrous β -CA (4.87 g; 25.1 mmol) and OX (1.13 g; 12.5 mmol) were dissolved in 7:2 (v/v) chloroform/methanol (90 mL) using heating reflux, then precipitation was performed under vacuum.

Caffeine:malonic acid, CA:MO: anhydrous β -CA (4.73 g; 24.4 mmol) and MO (1.27 g; 12.2 mmol) were dissolved in 30:1 (v/v) chloroform/methanol (50 mL) using heating reflux, then precipitation was performed under vacuum.

Caffeine:glutaric acid form II, CA:GL FII: anhydrous β -CA (3.57 g; 18.4 mmol) and GL (2.43 g; 18.4 mmol) were dissolved in chloroform (60 mL) using heating reflux, then precipitation was performed under vacuum.

Caffeine:glutaric acid form I, CA:GL FI: anhydrous β -CA (3.57 g; 18.4 mmol) and GL (2.43 g; 18.4 mmol) were dissolved in cyclohexane (90 mL) using heating reflux, then precipitation was performed under vacuum.

Caffeine:maleic, CA:ML (1:1): anhydrous β -CA (3.75 g; 19.3 mmol) and ML (2.25 g; 19.3 mmol) were dissolved in 4:1 (v/v) chloroform/methanol (50 mL), then precipitation was performed under vacuum.

CA:ML (2:1): anhydrous β -CA (4.62 g; 23.8 mmol) and ML (1.38 g; 11.9 mmol) were dissolved in 8:1 (v/v) chloroform/methanol (50 mL), then precipitation was performed by adding cyclohexane (1 mL) followed by n-hexane (20 mL), powder was collected after drying under vacuum.

Table S1: Prepared CA cocrystals, polymorphs, and their CCDC reference codes:

Cocrystal	Polymorph	CCDC code
CA:OX 2:1	Monoclinic, $P2_1/c$	GANXUP
CA:MO 2:1	Orthorhombic, $Fdd2$	GANYAW
CA:GL 1:1	Form II: Triclinic, $P\bar{1}$.	EXUQUJ
CA:GL 1:1	Form I: Monoclinic, $P2_1/c$.	EXUQUJ01
CA:ML 1:1	Form I: Monoclinic, $P2_1/n$	GANYEA
CA:ML 2:1	Monoclinic, Pc .	GANYIE01

2) Mixing Processes:

- Aqueous Processing:** Slurry formation was performed with an excess of cocrystal and a molar equivalent of SRD (2-4 g) in a glass vial containing deionised water (~5 ml). The slurry was mixed at ambient conditions using a magnetic stirrer for 24 hours. The resulting material was analysed using powder X-ray diffraction.
- Mechanical Processing:** It was performed by dry grinding. The cocrystal and molar equivalent of SRD cofomer mixture was ground using a Retsch MM200 ball mill, equipped with stainless steel 10-mL grinding jars and two 7-mm stainless steel grinding balls per jar. The grinding was performed at a rate of 25 Hz for a period of 90 minutes.

3) Thermogravimetric Analysis (TGA):

TGA was performed using a TGA Q500 from TA instruments. Approximately 2 to 4 mg of the sample was heated from 30 to 250 °C with a heat rate of 10 °C/min in an open standard titanium pan under nitrogen atmosphere. TGA data was analysed using the TA Universal analysis software version 4.5A.

4) Powder X-ray Diffraction (PXRD):

PXRD analysis was done using a Bruker D8 diffractometer with a Cu K α radiation source with a wavelength of 1.540 Å. The emission filament voltage and amperage were 40 kV and 40 mA, respectively. A scanning range of 4 to 40° 2 θ with a step size of 0.02° was used.

5) Equilibrium solubility determinations:

The saturation shaking flask method² was conducted by taking an excess of solid (3 g) to deionised water in a glass vial. The vials were shaken using a VWR 12L shaking water bath (UK), and the shaking was done for 24 h at 27 \pm 1 °C. pH readings were taken prior and after shaking using a Metler Toledo S220 Seven Compact™ pH meter. Samples were subjected to filtration and dilution prior to HPLC analysis. PXRD analysis was performed on the resulting solid to ensure that no physical transformation occurred during saturation.

6) High performance liquid chromatography (HPLC) analysis:

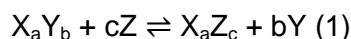
HPLC analysis was conducted using a Waters e-2695 separation module integrated with a degasser and a photodiode array detector (PDA-2998). The peaks were analysed with Empower 3 software. The column used was a Waters, Symmetry Shield™ Column, 5 μ m, and 4.6 x 100 mm. No guard column was used in this separation method. Analytes were detected at a wavelength of 205nm. All the chemicals used were laboratory grade and the mobile phase solvents were HPLC grade. All samples were analysed with a flow rate of 1.7 mL/min with an injection volume of 20 μ L. The column and samples were stored at 25 °C during the analysis. The mobile phase was composed of 25mM Potassium dihydrogen phosphate (pH=3) (solvent A) and methanol (solvent B) at a ratio of 88:12 A:B.

7) Density functional theory method:

The GRACE software package version 1.5.4³ was used to perform quantum mechanical DFT calculations of the lattice energies of CA, its cocrystals and the corresponding cofomers using the VASP program⁴ with a correction of the dispersive interaction⁵ (the DFT-D method). The starting geometry for each crystal was taken from the Cambridge Structural Database (CSD), Table S1. The DFT-D calculated lattice energies after geometry optimization were used to estimate the relative stability of a cocrystal in the presence of an additive.

8) Gibbs free energy change equation derivation:

This equation is used to calculate the Gibbs free energy change due to the solid state cofomer replacement reaction (Reaction 1):



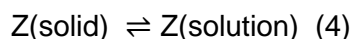
Considering the equilibrium solution reaction for each component of reaction (1) which are $X_a Y_b$, cZ , $X_a Z_c$, and bY , and considering that the thermodynamic activity of the solid is equal to one, solution equilibrium reactions and related ΔG° equations are:

For $X_a Y_b$:



$$\Delta G_{XY}^\circ = -RT \ln a_X^a a_Y^b = -RT \ln K_{sp}^{XY} \quad (3)$$

For Z:



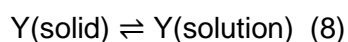
$$\Delta G_C^\circ = -RT \ln a'_Z \quad (5)$$

For $X_a Z_c$:



$$\Delta G_{XZ}^\circ = -RT \ln a_X^a a_Z^c = -RT \ln K_{sp}^{XZ} \quad (7)$$

For Y:



$$\Delta G_Y^\circ = -RT \ln a'_Y \quad (9)$$

By algebraically combining equilibrium reactions (2, 4, 6, and 8), reaction (1) is obtained. Similarly equations (3, 5, 7, and 9) can be combined to form a ΔG° equation (10) for cofomer replacement (ΔG_{Re}°). Since thermodynamic activities can be approximated by solubilities, pure solubilities of both cofomers S_C^Z and S_B^Y are used instead of thermodynamic activities.⁶

$$\Delta G_{\text{Re}}^{\circ} = -RT \ln \frac{K_{\text{sp}}^{\text{XY}} a_{\text{Z}}^{\text{c}}}{K_{\text{sp}}^{\text{XZ}} a_{\text{Y}}^{\text{b}}} = -RT \ln \frac{K_{\text{sp}}^{\text{XY}} S_{\text{Z}}^{\text{c}}}{K_{\text{sp}}^{\text{XZ}} S_{\text{Y}}^{\text{b}}} \quad (10)$$

Where K_{sp} is the solubility product of a cocrystal and S is the equilibrium solubility for a pure component. There are four possible general reactions in case of CA:DA coformer replacement with SRD, which depend primarily on the stoichiometry of the cocrystals involved:

Type 1: $\text{XY} + \text{Z} \rightleftharpoons \text{XZ} + \text{Y}$

Type 2: $\text{X}_2\text{Y} + \text{Z} \rightleftharpoons \text{X}_2\text{Z} + \text{Y}$

Type 3: $2\text{XY} + \text{Z} \rightleftharpoons \text{X}_2\text{Z} + 2\text{Y}$

Type 4: $\text{X}_2\text{Y} + \text{Z} \rightleftharpoons \text{XZ} + \text{Y} + \text{X}$

Equation (3) can be applied for all types, with a slight change in case of type 4 where CA solubility (S_{A}) is added:

$$\Delta G_{\text{Re}}^{\circ} = -RT \ln \frac{K_{\text{sp}}^{\text{XY}} S_{\text{Z}}^{\text{c}}}{K_{\text{sp}}^{\text{XZ}} S_{\text{Y}}^{\text{b}} S_{\text{X}}} \quad (4)$$

Solubilities and solubility products of pure components and cocrystals, respectively, were determined using the shaking flask method followed by HPLC analysis methods (see sections 5 and 6)

Supporting Results:

9) Characterisation of prepared cocrystals by PXRD:

Cocrystals were successfully prepared with good crystallinity; PXRD patterns are shown in Figure S1.

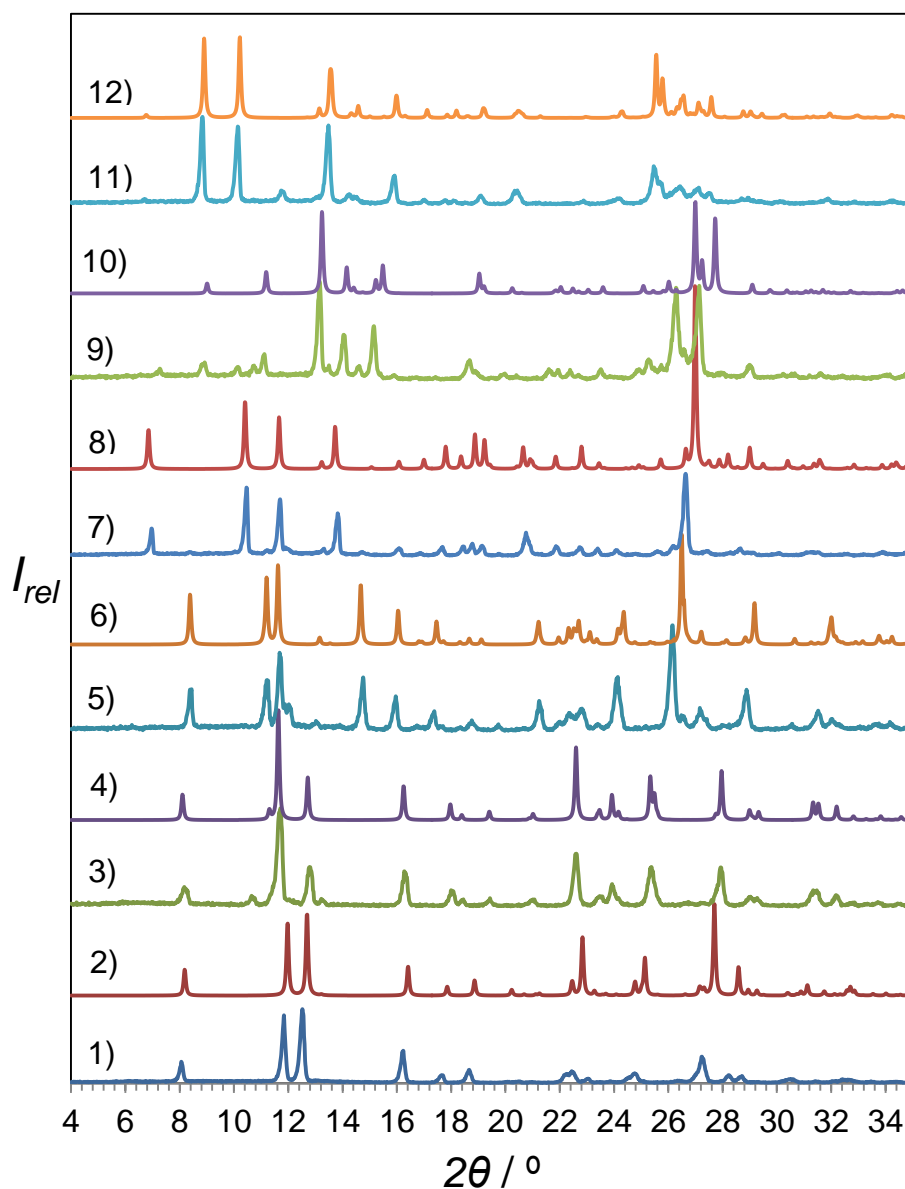


Figure S1: PXRD patterns for: 1) Exp CA:OX, 2) Sim** CA:OX, 3) Exp CA:MO, 4) Sim CA:MO, 5) Exp CA:GL FII, 6) Sim CA:GL FII, 7) Exp CA:GL FI, 8) Sim CA:GL FI, 9) Exp CA:ML 1:1, 10) Sim CA:ML 1:1, 11) Exp CA:ML 2:1, and 12) Sim CA:ML 2:1. Exp = Experimental result of solution crystallization method, ** Sim = simulated pattern.

10) Aqueous processing reactions:

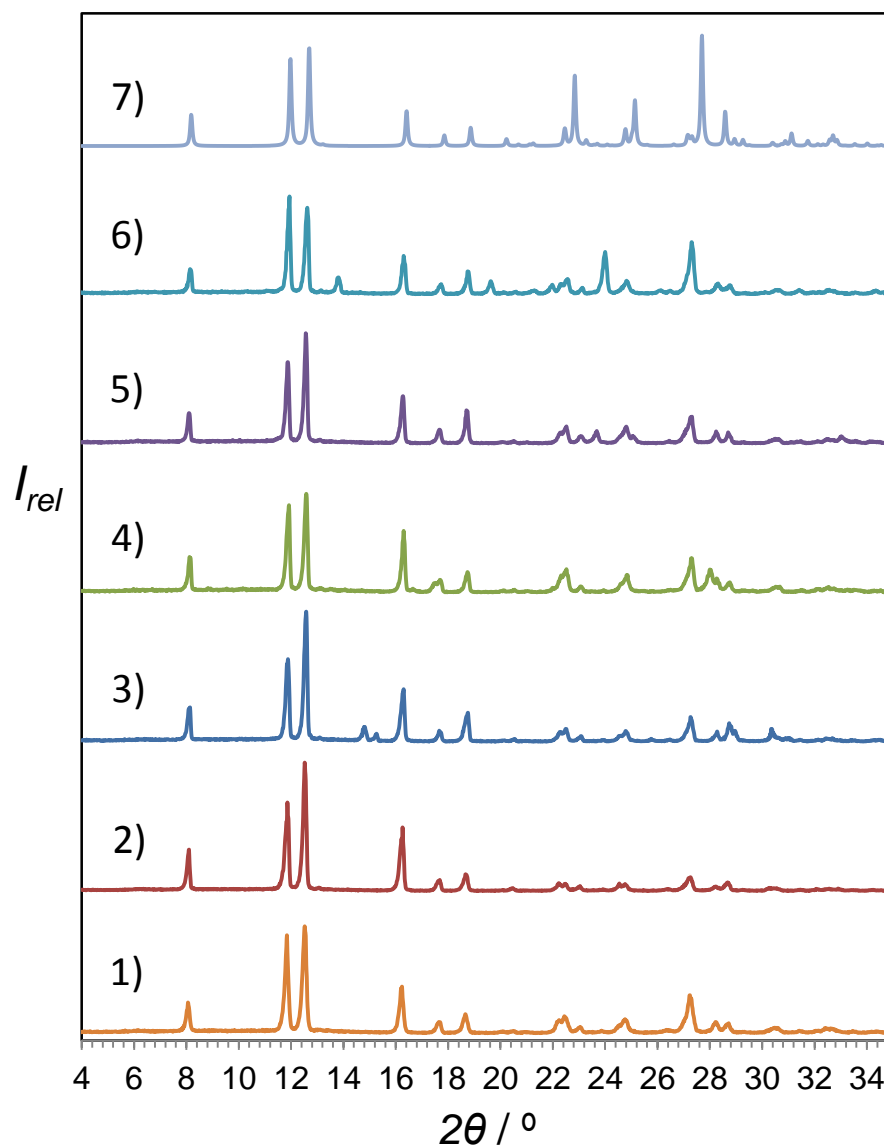


Figure S2: PXR D patterns for CA:OX 2:1 after aqueous processing in the presence of SRDs: 1) experimental CA:OX 2:1, 2) CA:OX 2:1 slurry, 3) CA:OX 2:1 + ML slurry, 4) CA:OX 2:1 + GL slurry, 5) CA:OX 2:1 + MO slurry, 6) CA:OX 2:1 + OX slurry, and 7) sim CA:OX 2:1. This shows how CA:OX 2:1 sustained its structure in the presence of all SRDs after slurring for 24 h.

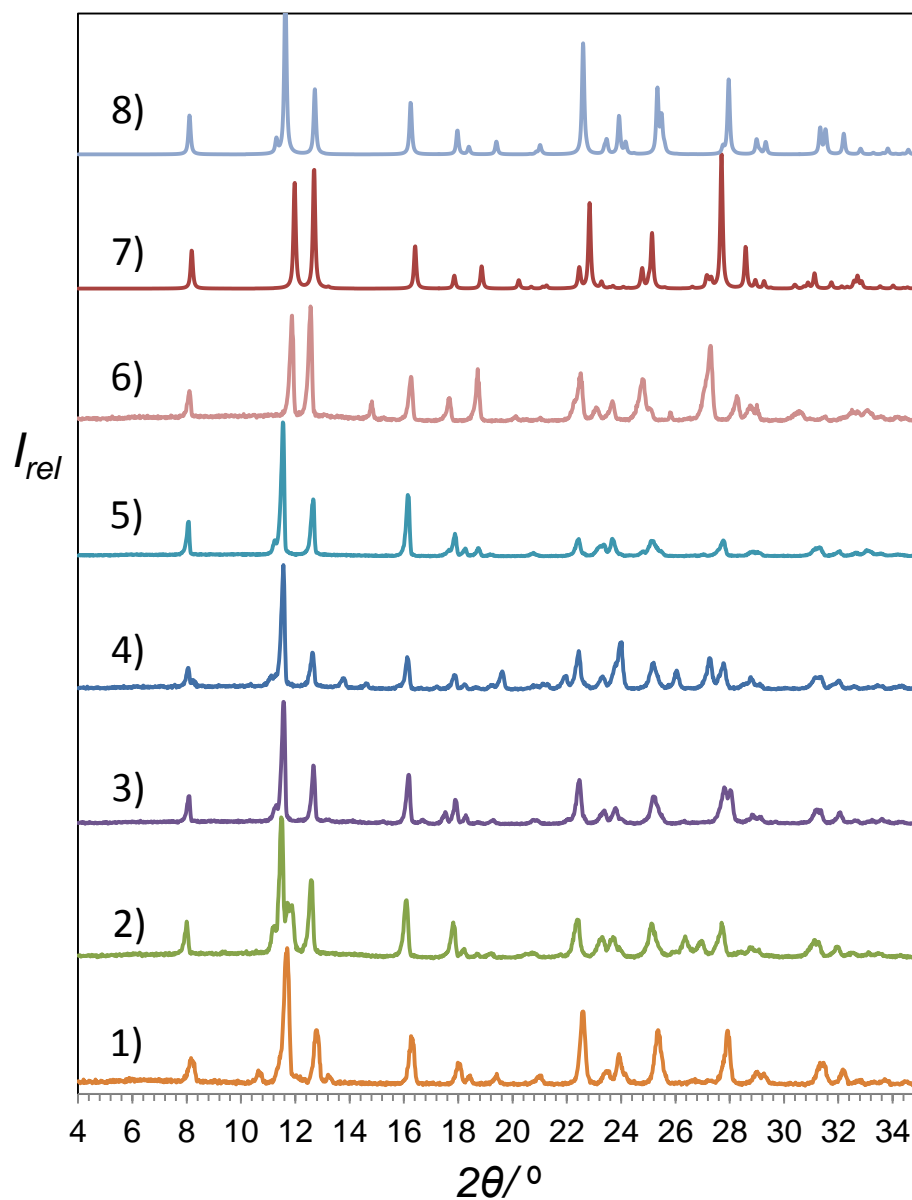


Figure S3. PXRD patterns for CA:MO after aqueous processing in the presence of SRDs: 1) experimental CA:MO, 2) CA:MO slurry, 3) CA:MO + ML slurry, 4) CA:MO + GL slurry, 5) CA:MO + MO slurry, 6) simulated CA:MO, 7) CA:MO + OX slurry, and 8) simulated CA:OX. This shows how CA:MO sustained its structure in the presence of all SRDs after slurring for 24 h except OX were the pattern changed to CA:OX.

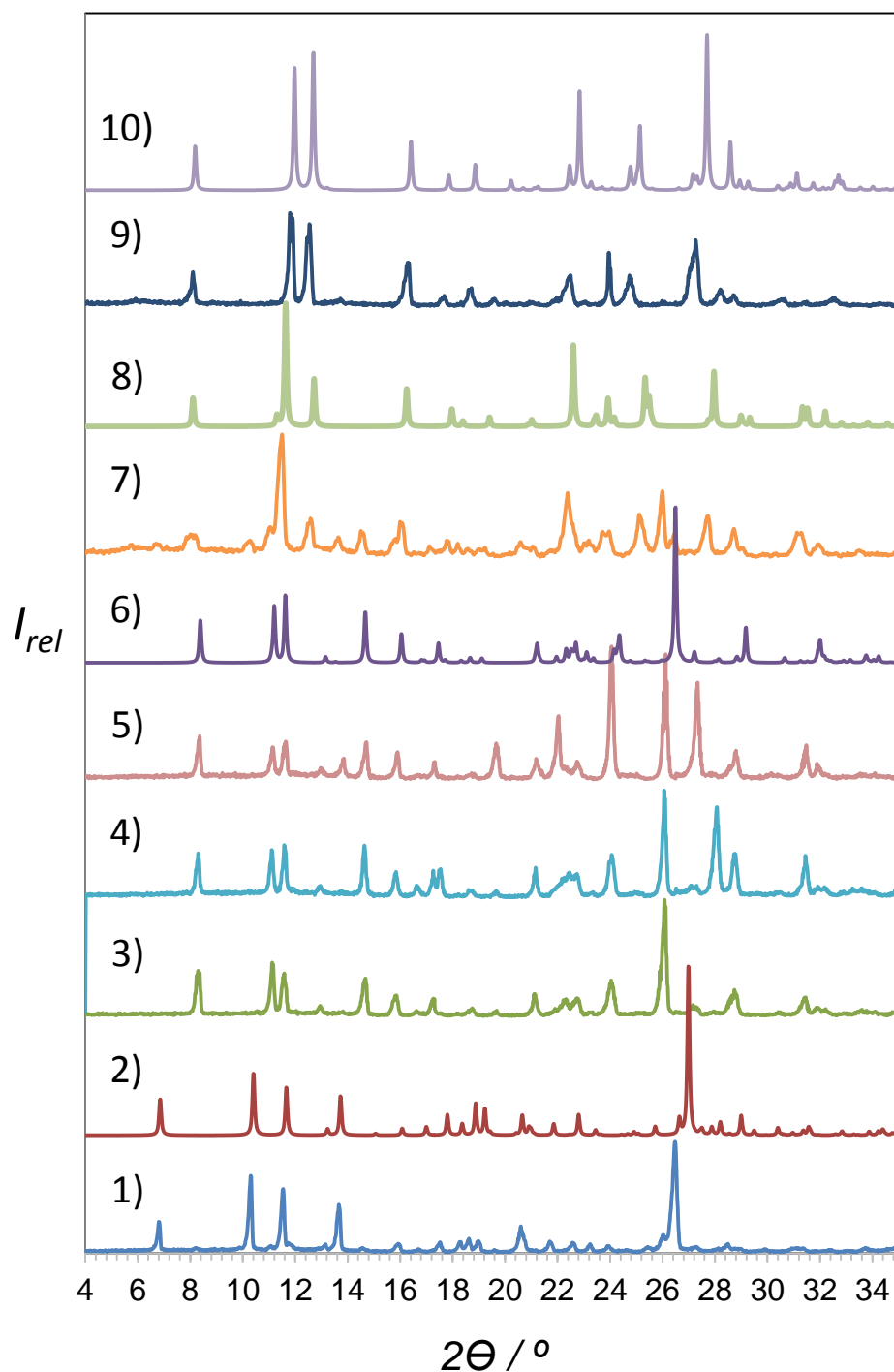


Figure S4. PXRD patterns for CA:GL FI after aqueous processing in the presence of SRDs: 1) experimental CA:GL FI, 2) simulated CA:GL FI, 3) CA:GL FI slurry, 4) CA:GL FI + ML slurry, 5) CA:GL FI + GL slurry, 6) simulated CA:GL FII, 7) CA:GL FI + MO slurry, 8) simulated CA:MO, 9) CA:GL FI + OX slurry, and 10) simulated CA:OX. CA:GL FI undergoes polymorphic transformation to FII when slurried alone or in the presence of ML or GL. Moreover, cofomer replacement is observed after slurrying in the presence of MO or OX.

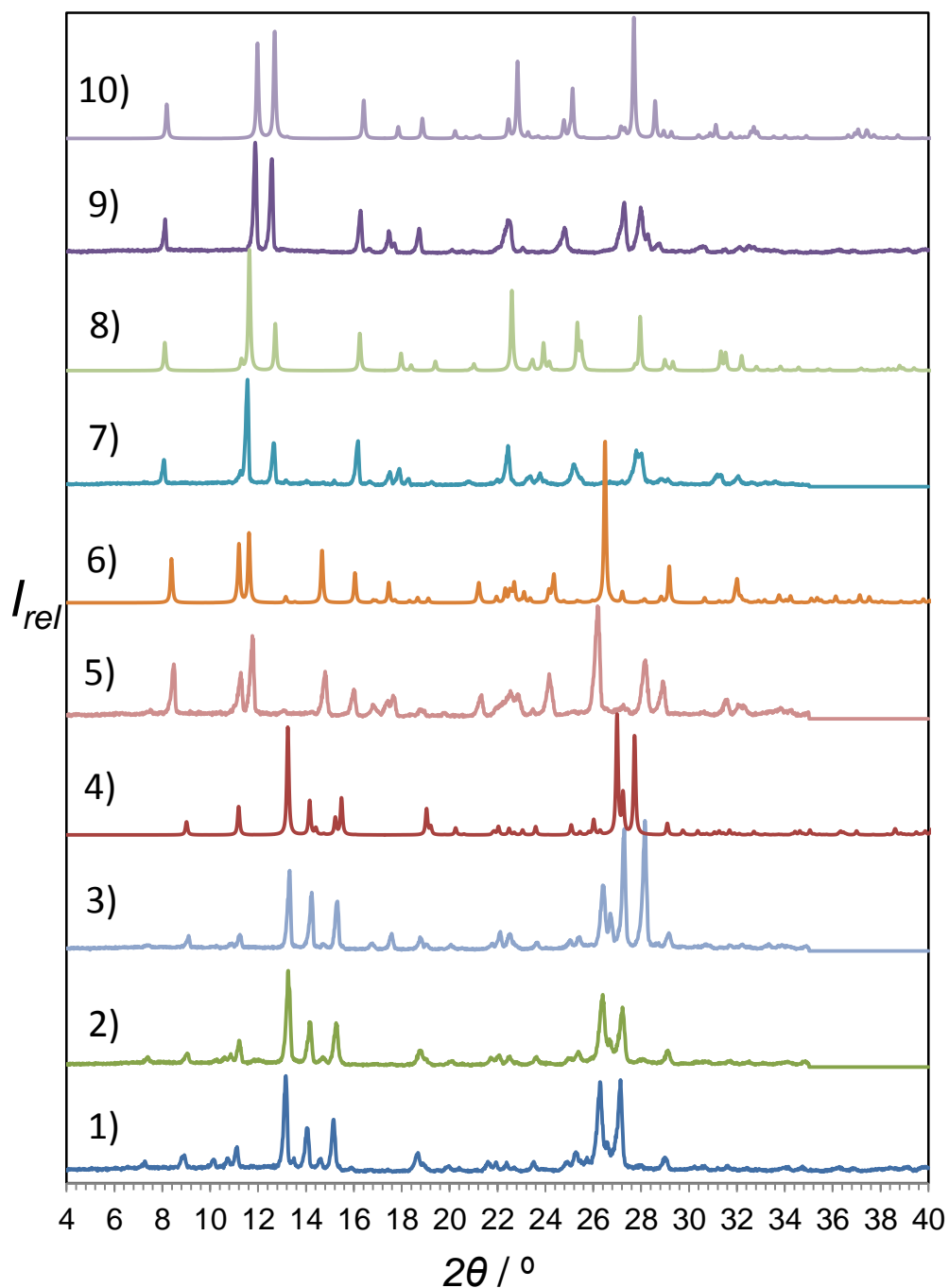


Figure S5. PXR D patterns for CA:ML 1:1 after aqueous processing in the presence of SRDs: 1) experimental CA:ML 1:1, 2) CA:ML 1:1 slurry, 3) CA:ML 1:1 + ML slurry, 4) simulated CA:ML 1:1, 5) CA:ML 1:1 + GL slurry, 6) simulated CA:GL FII, 7) CA:ML 1:1 + MO slurry, 8) simulated CA:MO, 9) CA:ML 1:1 + OX slurry, and 10) simulated CA:OX. CA:ML 1:1 undergoes coformer replacement after slurrying in the presence of GL, MO, or OX. No transformation is observed when slurried alone or in the presence of ML.

11) Mechanical processing reactions:

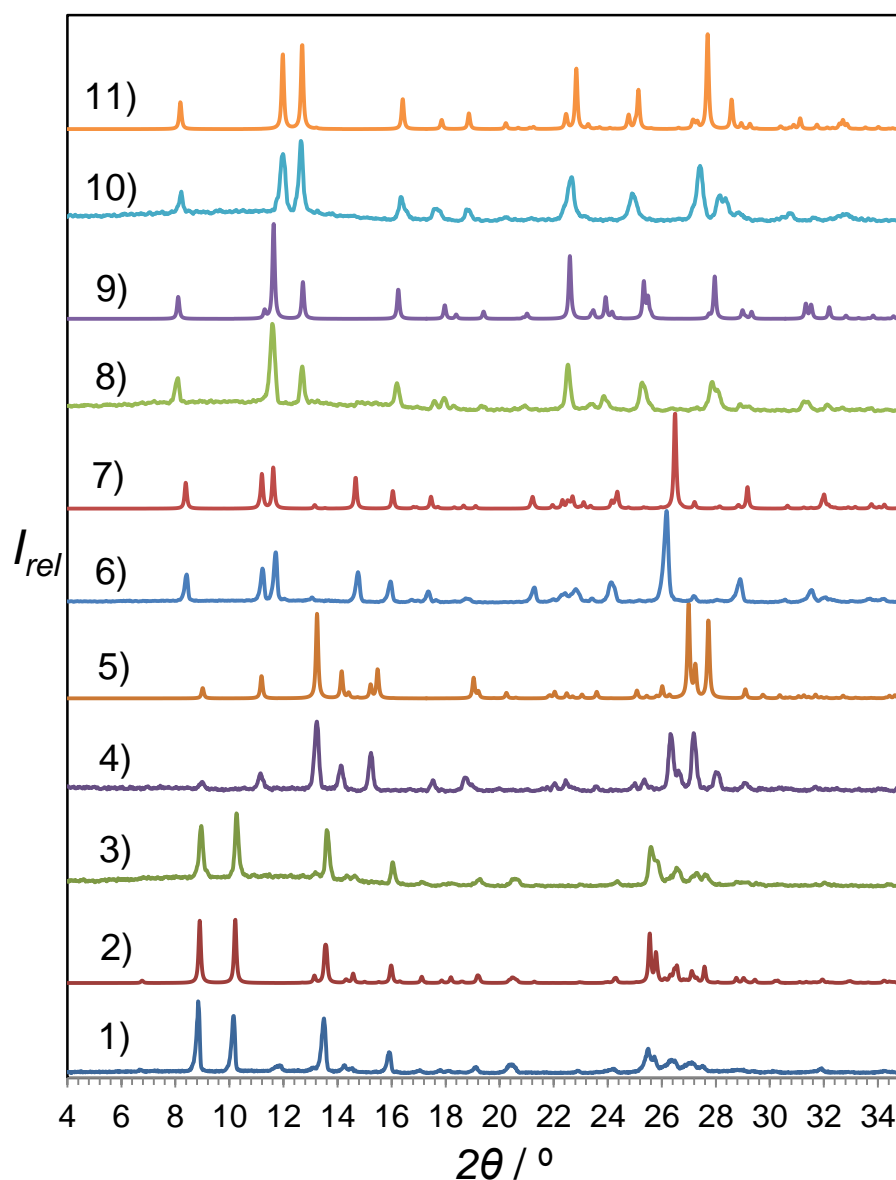


Figure S6: PXRD patterns for CA:ML 2:1 after mechanical processing in the presence of SRDs: 1) Exp CA:ML 2:1, 2) sim CA:ML 2:1, 3) CA:ML 2:1 grind, 4) CA:ML 2:1 + ML grind, 5) sim CA:ML 1:1, 6) CA:ML 2:1 + GL grind, 7) sim CA:GL FII, 8) CA:ML 2:1 + MO grind, 9) sim CA:MO, 10) CA:ML 2:1 + OX grind, and 11) sim CA:OX. CA:ML 2:1 undergoes coformer replacement by OX, MO, or GL during mechanical processing. Moreover, it is subjected to stoichiometric conversion in the presence of additional ML.

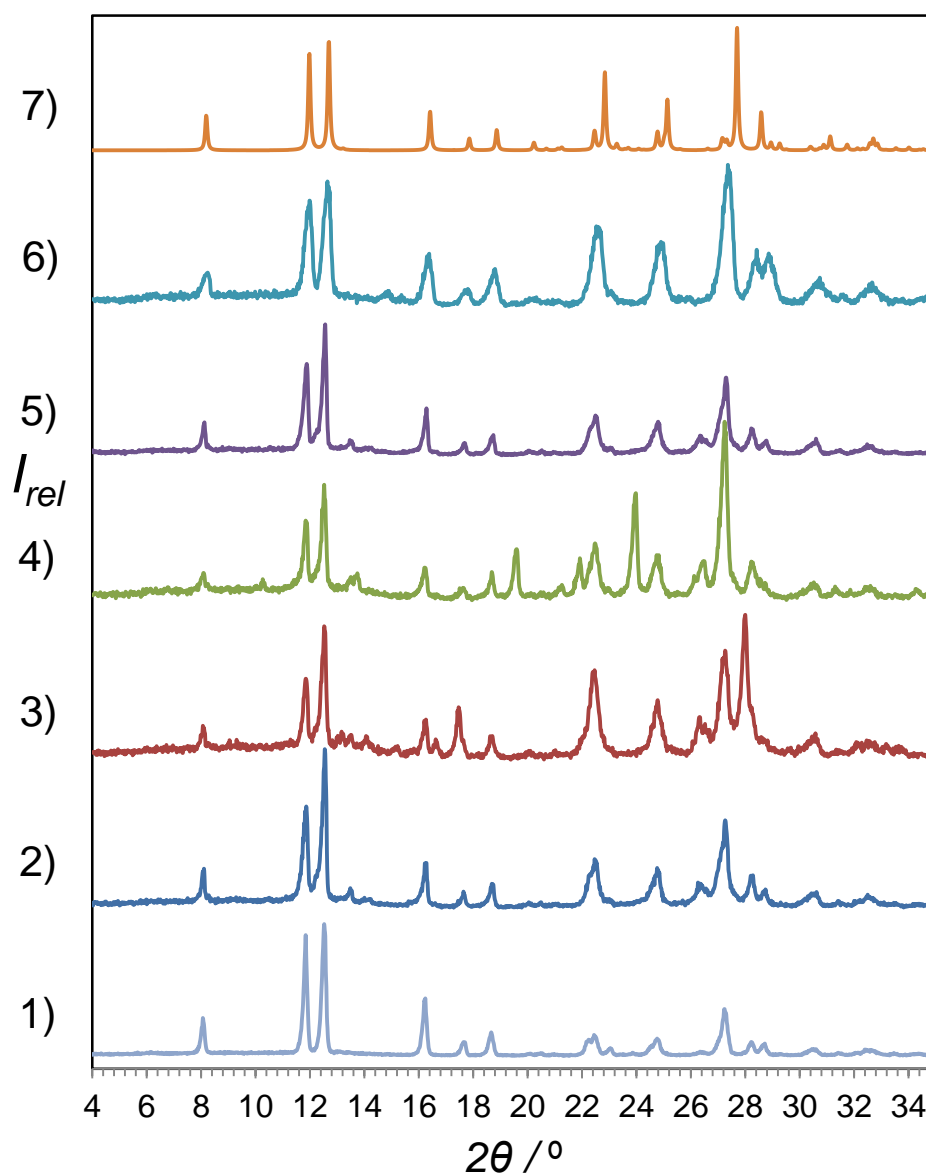


Figure S7: PXR D patterns for CA:OX after mechanical processing in the presence of SRDs: 1) Exp CA:OX, 2) CA:OX grind, 3) CA:OX + ML grind, 4) CA:OX + GL grind, 5) CA:OX + MO grind, 6) CA:OX + OX grind, and 7) sim CA:OX. CA:OX is resistant to coformer replacement by other SRDs during mechanical processing.

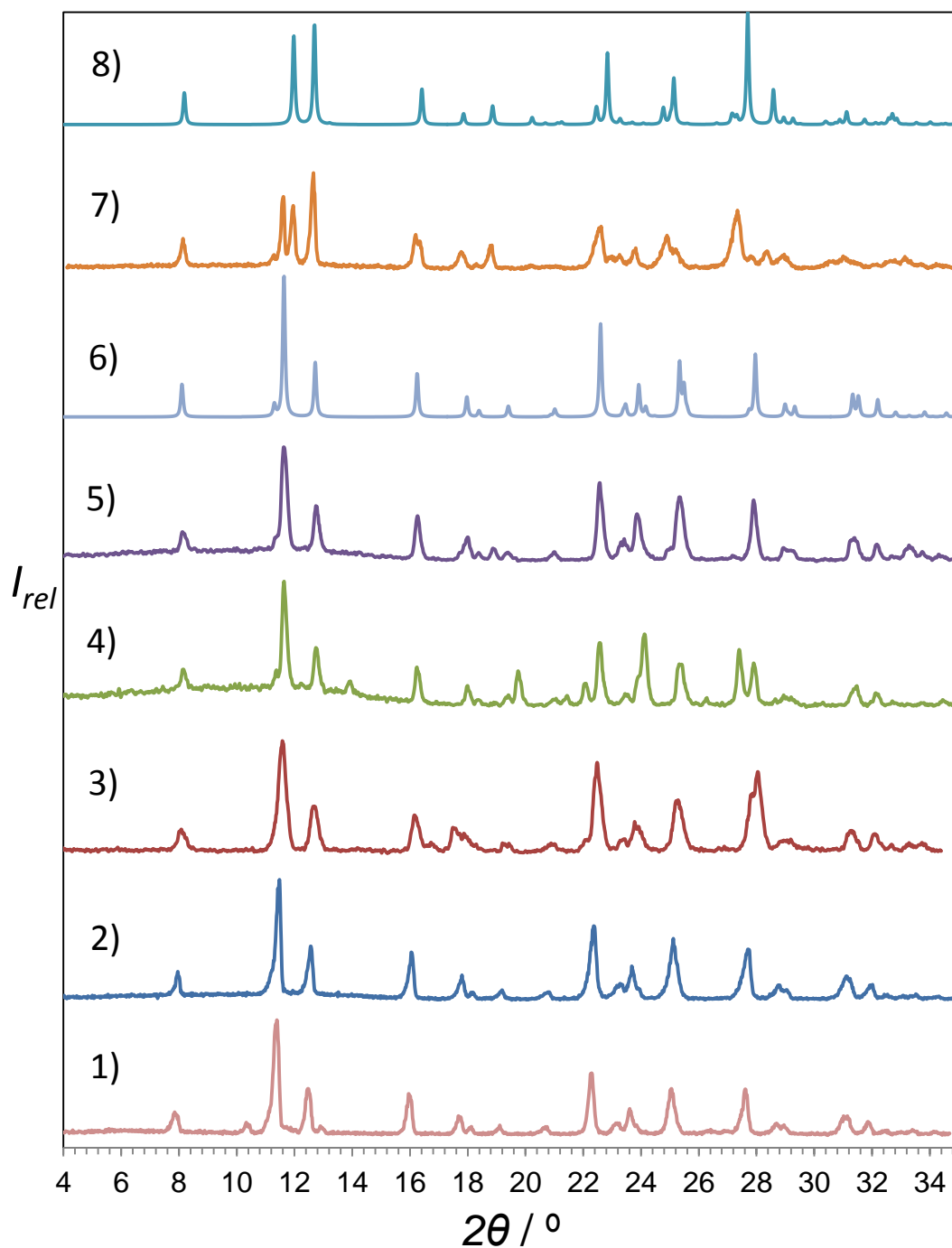


Figure S8. PXRD patterns for CA:MO after mechanical processing in the presence of SRDs: 1) experimental CA:MO, 2) CA:MO grind, 3) CA:MO + ML grind, 4) CA:MO + GL grind, 5) CA:MO + MO grind, 6) simulated CA:MO, 7) CA:MO + OX grind, and 8) simulated CA:OX. Similar to aqueous processing, mechanical processing of CA:MO in the presence of OX has caused coformer replacement. Moreover, the presence of other SRDs has not caused any change.

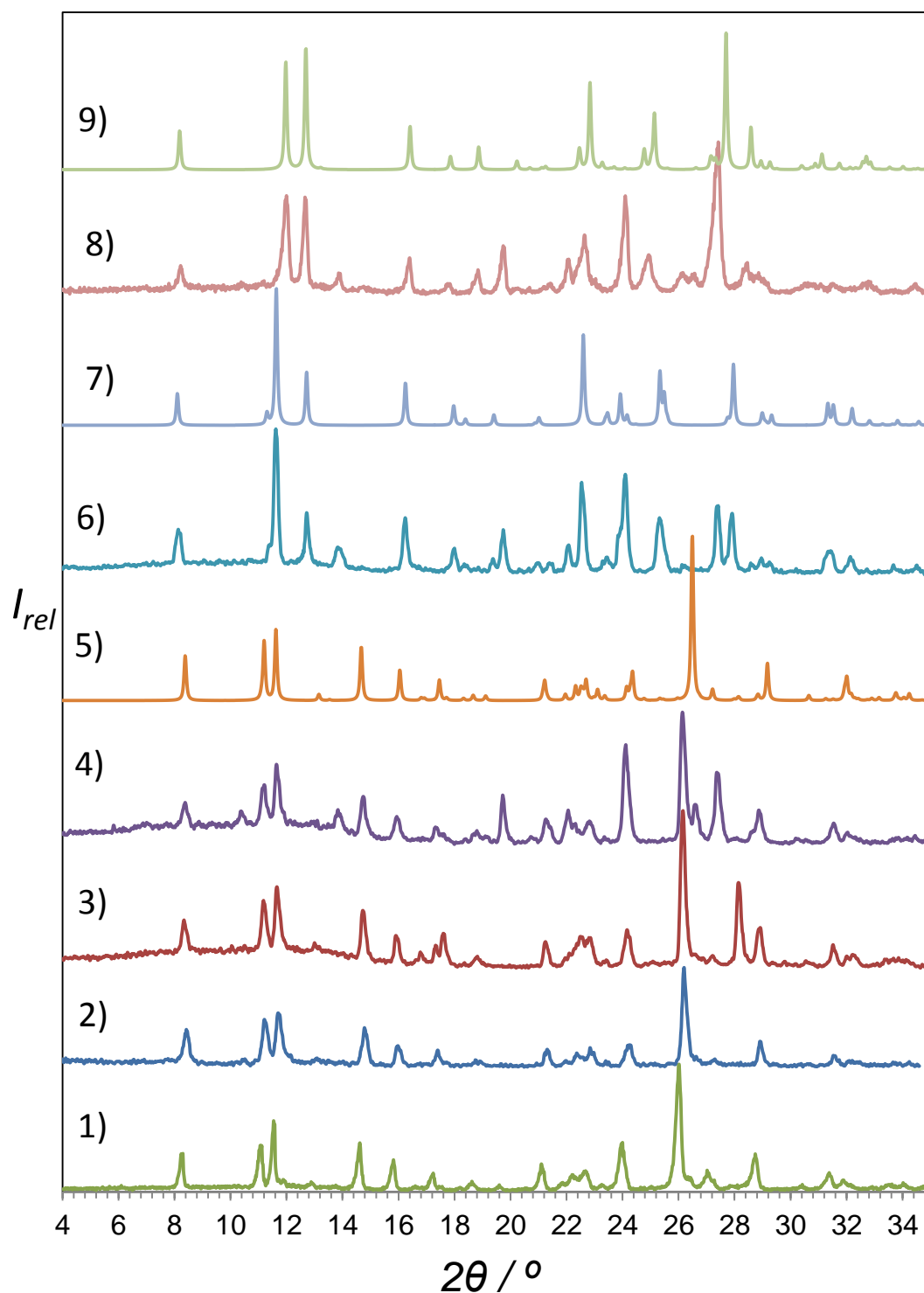


Figure S9. PXRD patterns for CA:GL FII after mechanical processing in the presence of SRDs: 1) experimental CA:GL FII 2) CA:GL FII grind, 3) CA:GL FII + ML grind, 4) CA:GL FII + GL grind, 5) simulated CA:GL FII, 6) CA:GL FII + MO grind, 7) simulated CA:MO, 8) CA:GL FII + OX grind, and 9) simulated CA:OX. Both OX or MO can induce coformer replacement if present during mechanical processing of CA:GL FII. However, CA:GL FII resists replacement and sustains its structure during mechanical processing alone or in the presence of ML or GL.

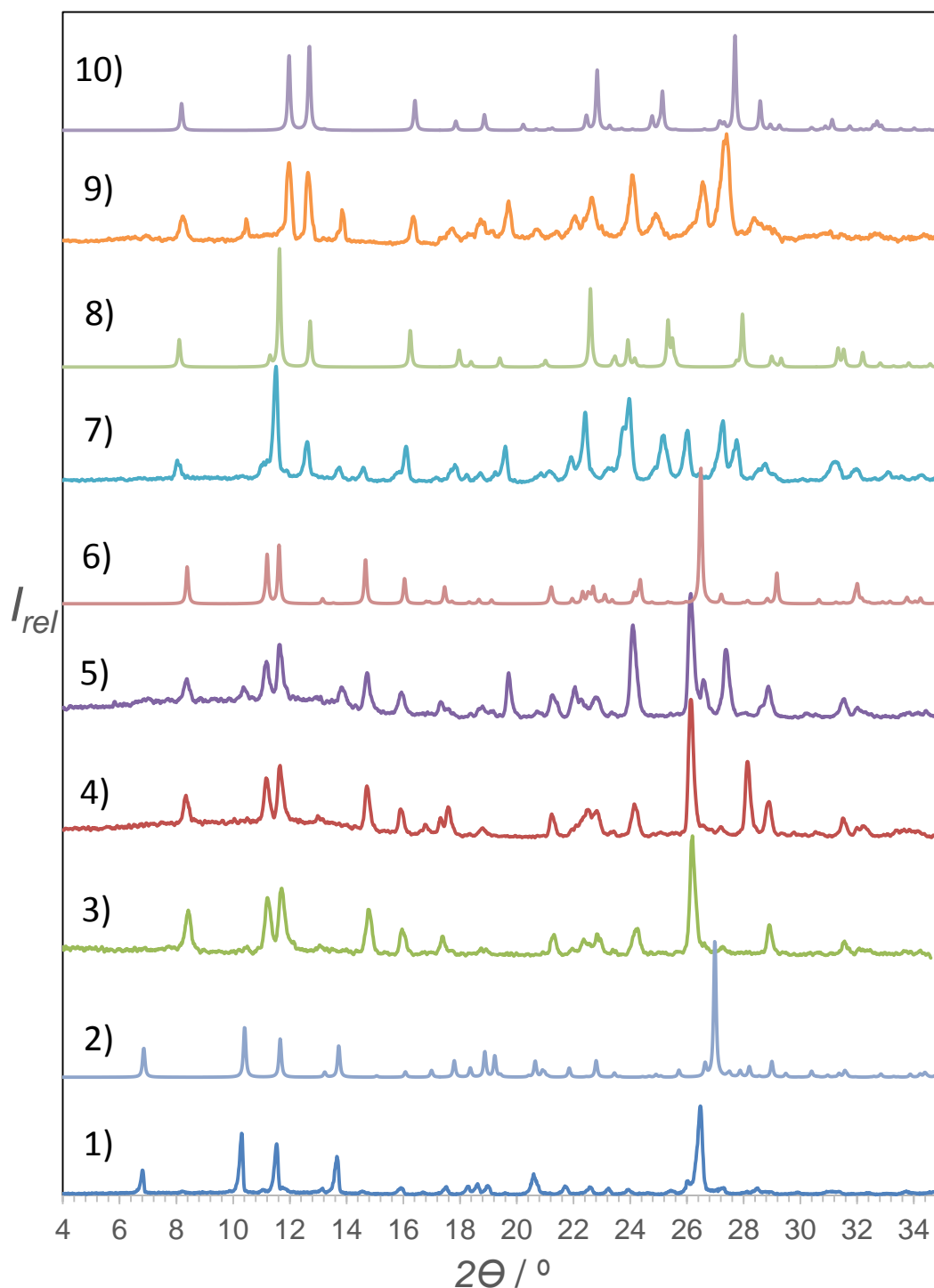


Figure S10. PXR D patterns for CA:GL FI after mechanical processing in the presence of SRDs: 1) experimental CA:GL FI, 2) simulated CA:GL FI, 3) CA:GL FI grind, 4) CA:GL FI + ML grind, 5) CA:GL FI + GL grind, 6) simulated CA:GL FII, 7) CA:GL FI + MO grind, 8) simulated CA:GL, 9) CA:GL FI + OX grind, and 10) simulated CA:OX. CA:GL FI exhibits polymorphic transformation after mechanical processing alone or in the presence of ML or GL as SRDs. In addition, the presence of MO or OX during activation leads to coformer replacement.

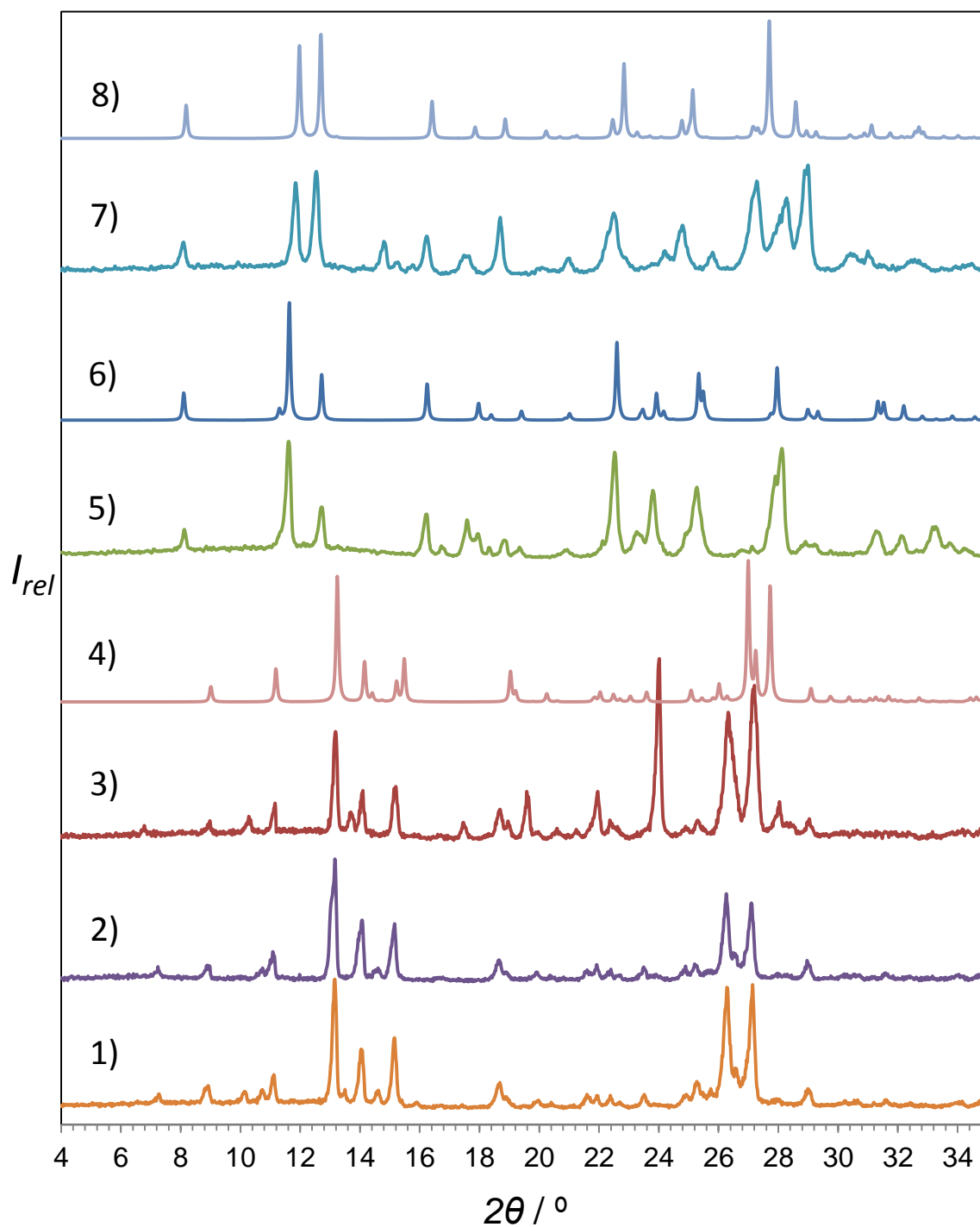


Figure S11. PXRD patterns for CA:ML 1:1 after mechanical processing in the presence of SRDs: 1) experimental CA:ML 1:1, 2) CA:ML 1:1 + ML grind, 3) CA:ML 1:1 + GL grind, 4) simulated CA:ML 1:1, 5) CA:ML 1:1 + MO grind, 6) simulated CA:MO, 7) CA:ML 1:1 + OX grind, and 8) simulated CA:OX. CA:ML 1:1 exhibits no physical transformation after mechanical processing alone or in the presence of ML or GL. However, cofomer replacement is observed in the presence of MO or OX.

12) Thermal gravimetric analysis (TGA):

Sample: CAF:OXA
Size: 1.7470 mg
Method: Ramp

TGA

File: C:\...\PhD\Results\TGA\GRIND\CAF-OXA.001
Operator: Bashir
Run Date: 16-Dec-2015 15:58
Instrument: TGA Q5000 V3.17 Build 265

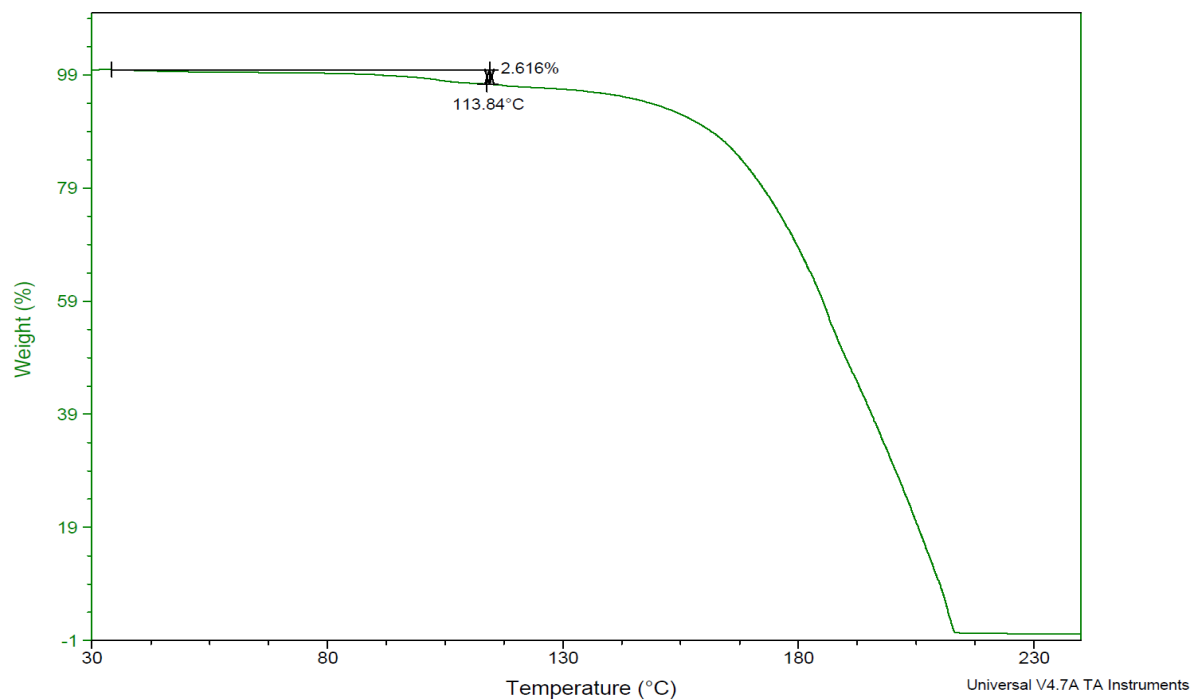


Figure S12: TGA thermogram of CA:OX cocrystal.

Sample: CAF:MOA
Size: 2.6590 mg
Method: Ramp

TGA

File: C:\...\PhD\Results\TGA\GRIND\CAF-MOA.001
Operator: Bashir
Run Date: 16-Dec-2015 14:54
Instrument: TGA Q5000 V3.17 Build 265

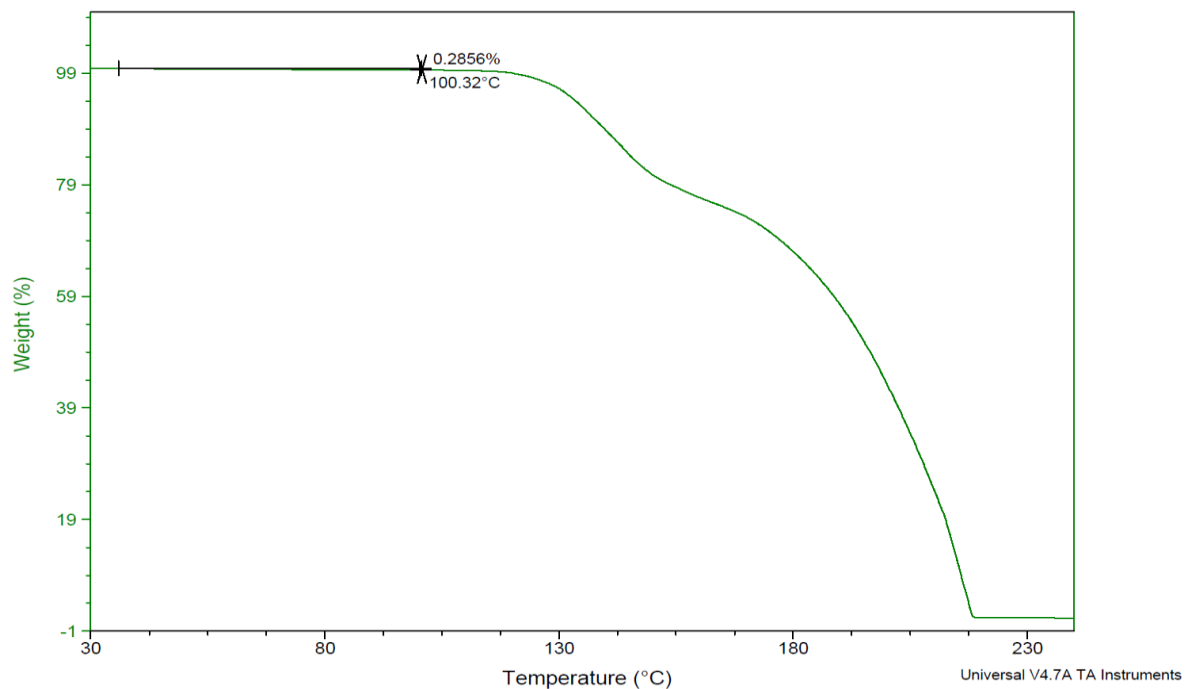


Figure S13: TGA thermogram of CA:MO cocrystal.

Sample: CG FII
Size: 3.6580 mg
Method: Ramp

TGA

File: E:\TGA\CG FII.001
Operator: BASHIR
Run Date: 30-Jul-2015 19:44
Instrument: TGA Q5000 V3.17 Build 265

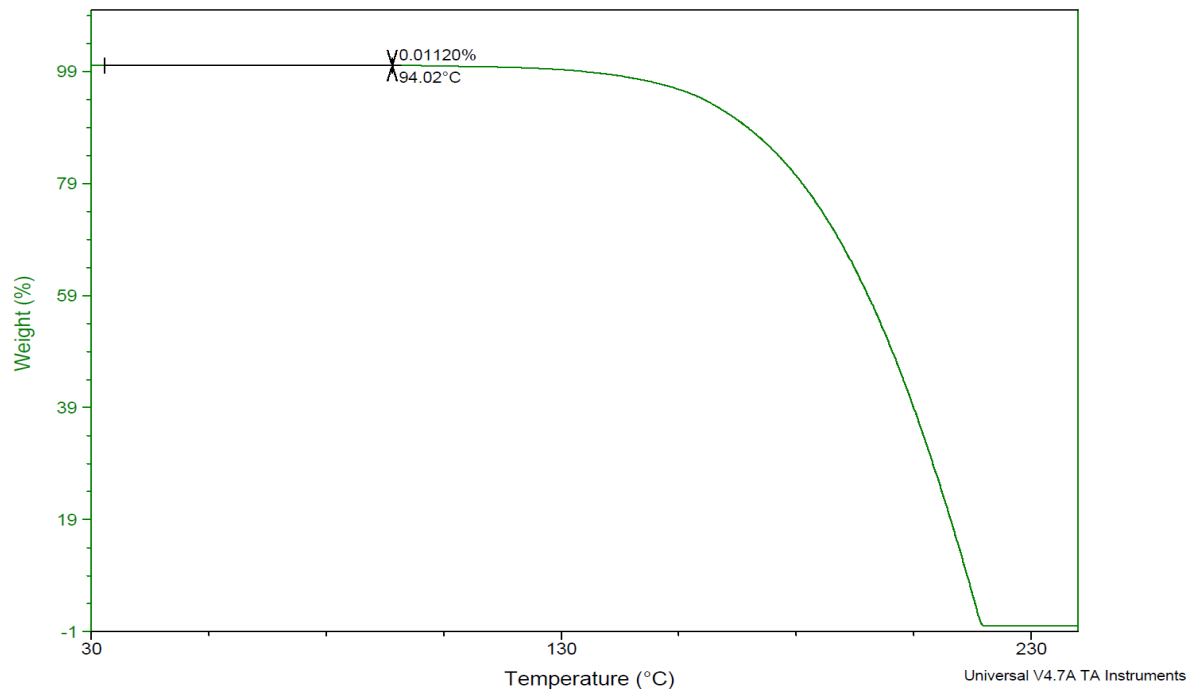


Figure S14: TGA thermogram of CA:GL FII cocrystal.

Sample: CG FI
Size: 2.3010 mg
Method: Ramp

TGA

File: E:\TGA\CG FI.001
Operator: BASHIR
Run Date: 30-Jul-2015 20:37
Instrument: TGA Q5000 V3.17 Build 265

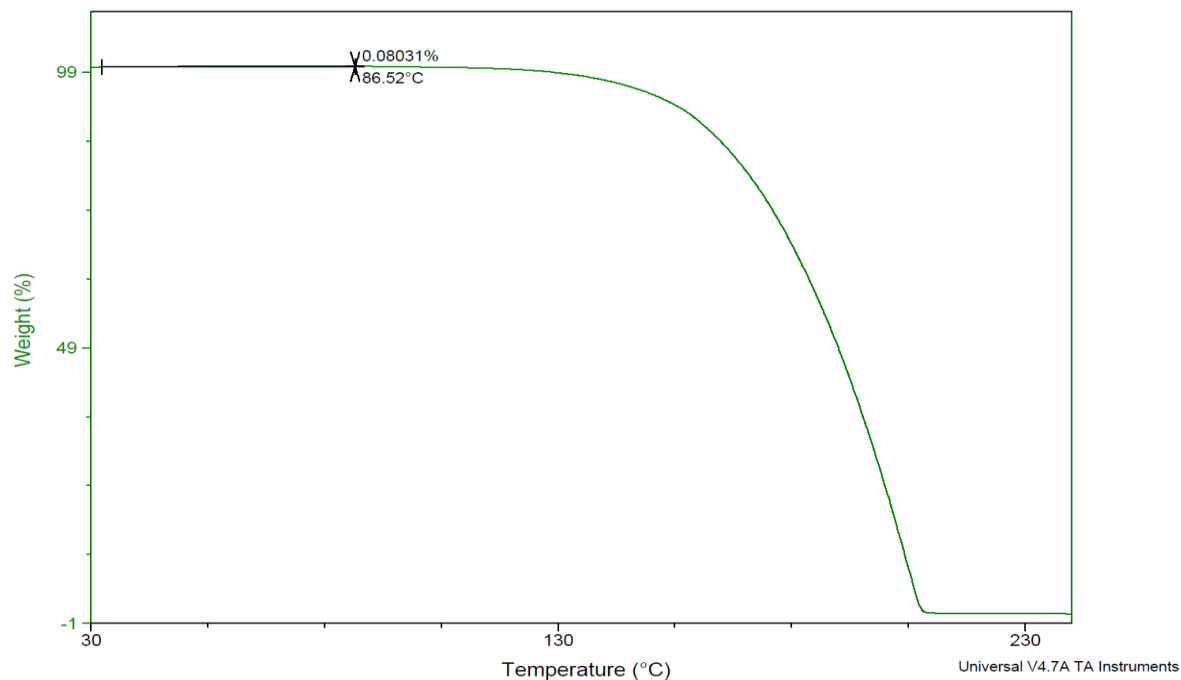


Figure S15: TGA thermogram of CA:GL FI cocrystal.

Sample: CAF-MLA 1-1
Size: 2.7790 mg
Method: Ramp

TGA

File: C:\...Results\TGA\GRIND\CAF-MLA 1-1.001
Operator: Bashir
Run Date: 16-Dec-2015 15:21
Instrument: TGA Q5000 V3.17 Build 265

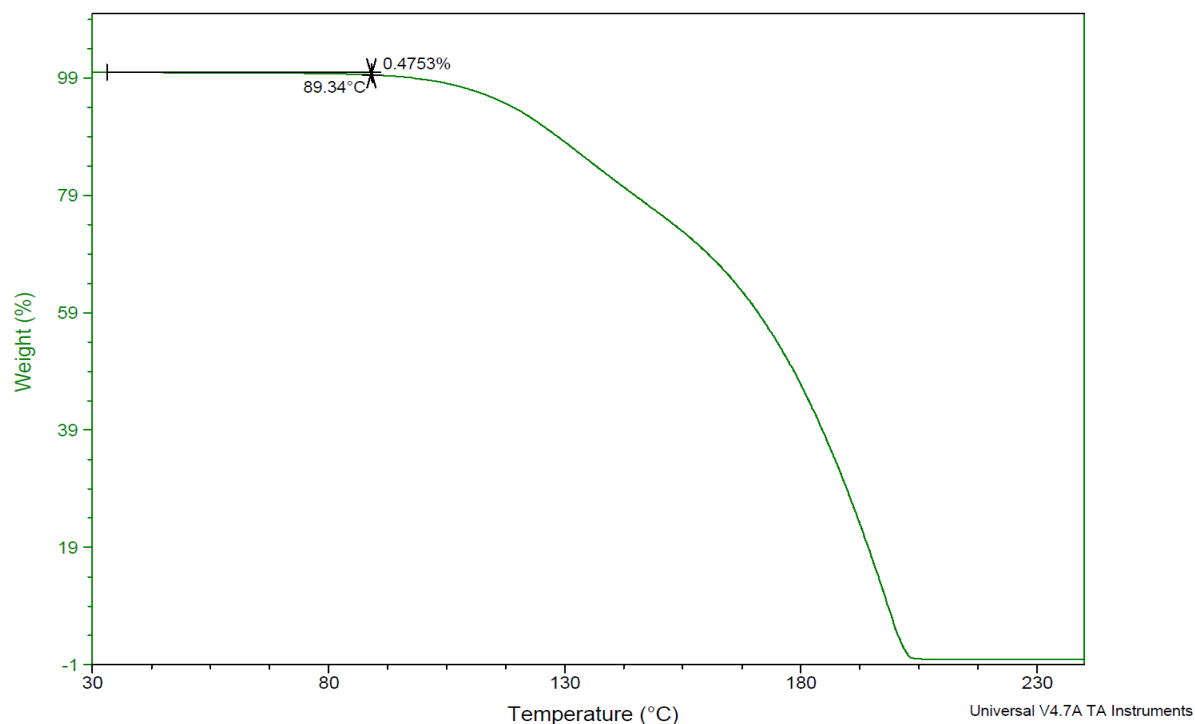


Figure S16: TGA thermogram of CA:ML 1:1 cocrystal.

Sample: Caf:Mal 2:1
Size: 1.2120 mg
Method: Ramp
Comment: 1st

TGA

File: C:\...PhD\Results\TGA\Caf-Mal 2-1.001
Operator: MBS
Run Date: 17-Jan-2015 22:25
Instrument: TGA Q5000 V3.17 Build 265

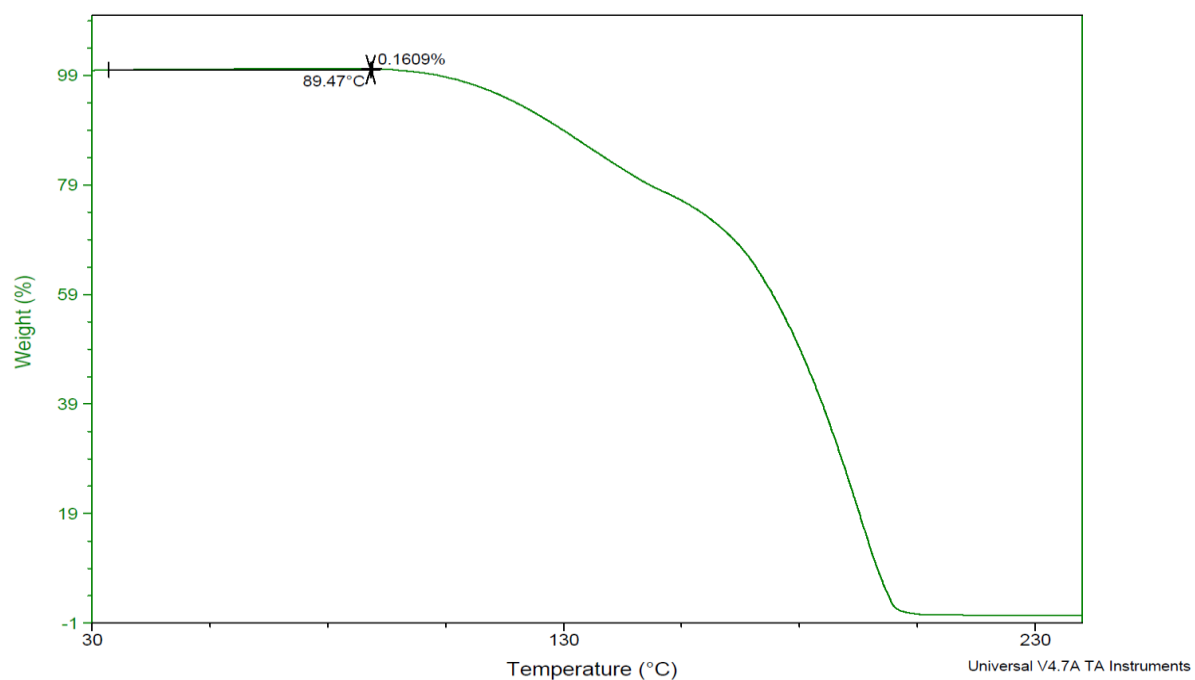


Figure S17: TGA thermogram of CA:ML 2:1 cocrystal.

Sample: OXA
Size: 4.2210 mg
Method: Ramp

TGA

File: C:\...PhD\Results\TGA\GRIND\OXA.001
Operator: Bashir
Run Date: 16-Dec-2015 13:05
Instrument: TGA Q5000 V3.17 Build 265

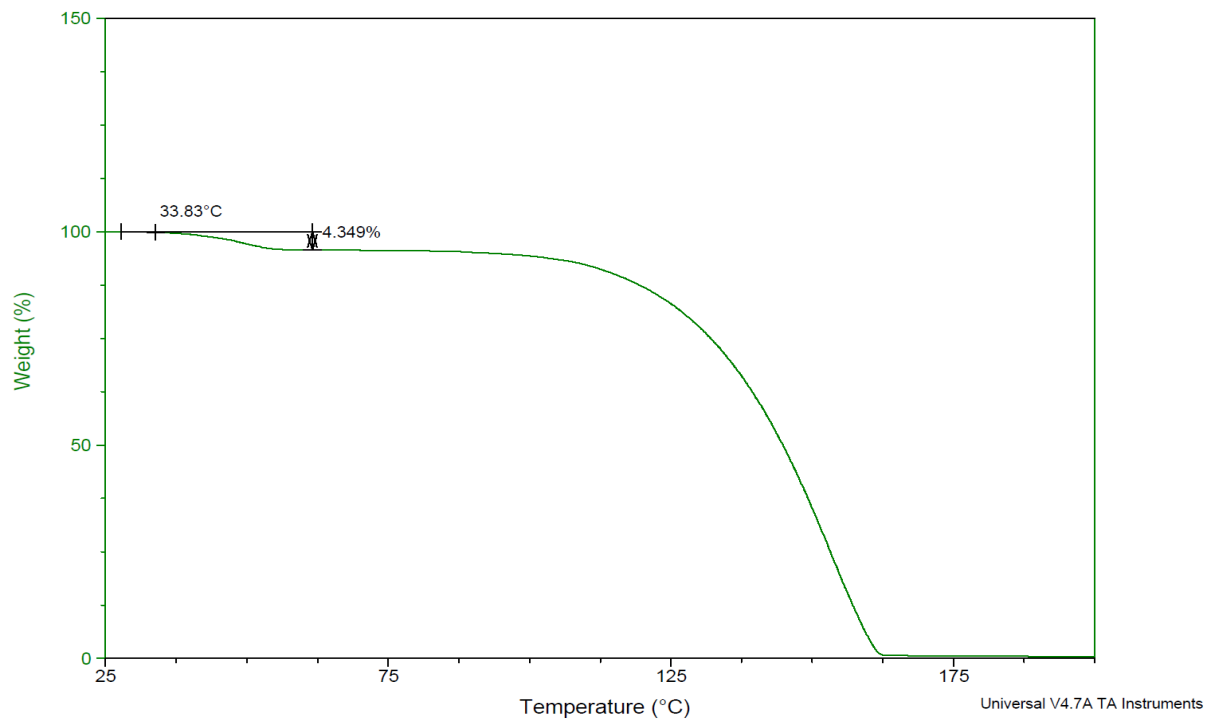


Figure S18: TGA thermogram of OX.

Sample: MOA
Size: 5.0770 mg
Method: Ramp

TGA

File: C:\...PhD\Results\TGA\GRIND\MOA.001
Operator: Bashir
Run Date: 16-Dec-2015 13:33
Instrument: TGA Q5000 V3.17 Build 265

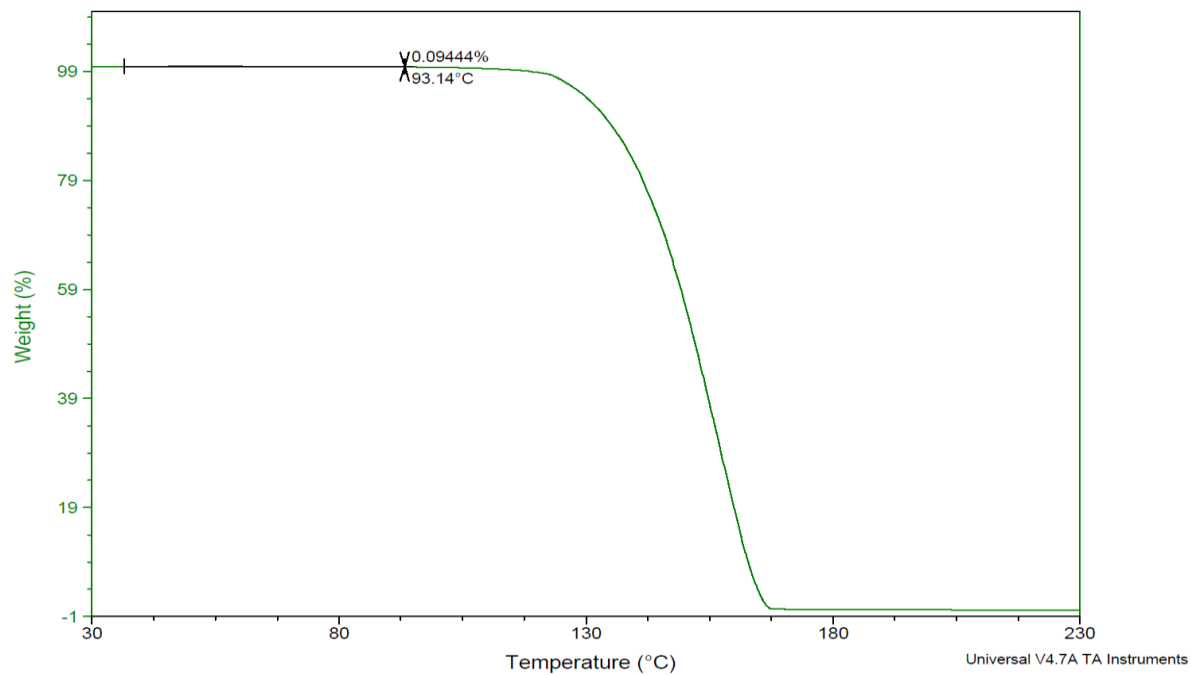


Figure S19: TGA thermogram of MO.

Sample: GLA
Size: 6.0460 mg
Method: Ramp

TGA

File: C:\...PhD\Results\TGA\GRIND\GLA.001
Operator: Bashir
Run Date: 16-Dec-2015 14:27
Instrument: TGA Q5000 V3.17 Build 265

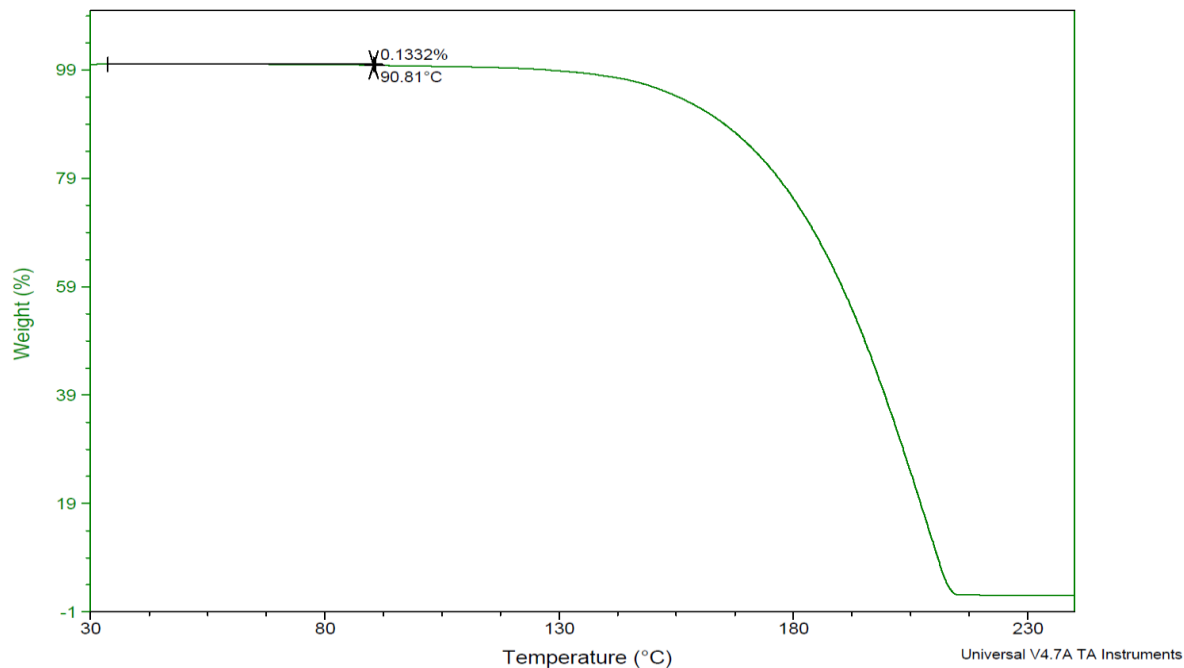


Figure S20: TGA thermogram of GL.

Sample: MLA
Size: 5.5070 mg
Method: Ramp

TGA

File: C:\...PhD\Results\TGA\GRIND\MLA.002
Operator: Bashir
Run Date: 16-Dec-2015 14:00
Instrument: TGA Q5000 V3.17 Build 265

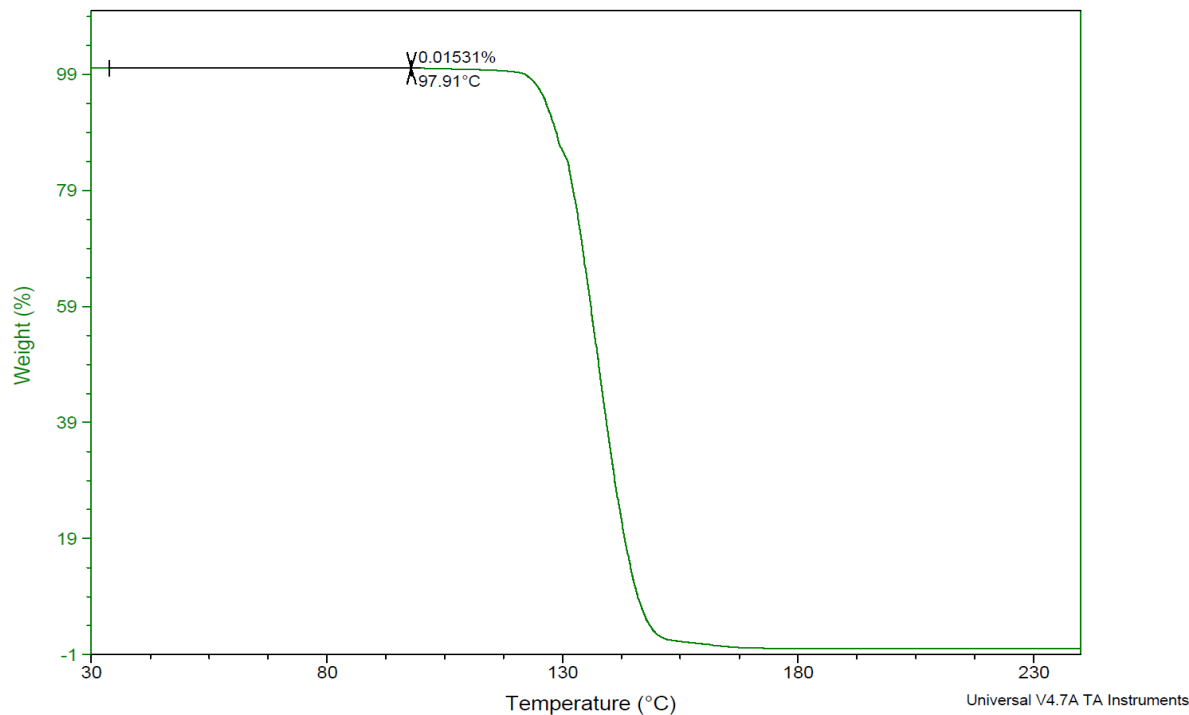


Figure S21: TGA thermogram of ML.

13) DFT Computational data:

Lattice energy calculation results are presented in Tables S2, S3 and S4. Lattice energies of the most stable polymorph (Table S3) for each molecule were used to calculate the relative stabilities of the cocrystals (Table S4). In the case of caffeine it should be pointed out that we have used the optimised lattice energy of its most stable polymorph for the calculation of the stabilities of the co-crystal. At room temperature, caffeine is known to possess some disorder⁷ but our choice is consistent with our overall approach which ignores temperature effects.

Table S2: Optimized unit cell parameters and their deviations from experimental determinations.

CCDC Reference code	Crystal	Optimized Cell						Percentage Error ^[a]					
		a/Å	b/Å	c/Å	α/deg	β/deg	γ/deg	a	b	c	α	β	γ
NIWFEE03 ⁸	CA	8.34	8.62	11.39	68.5	78.3	73.5	0.2	-0.6	0.2	-0.6	-0.4	-1.1
GLURAC06 ⁹	GL α-form	13.01	6.62	17.02	90.0	98.5	90.0	0.0	0.3	-0.7	0.0	0.6	0.0
GLURAC08 ¹⁰	GL β-form	4.47	14.63	15.82	90.0	96.4	90.0	1.2	-0.9	-0.6	0.0	-0.1	0.0
MALIAC12 ¹¹	ML P2 ₁ /c	30.42	31.21	4.67	90.0	90.0	90.0	0.1	-0.2	0.0	0.0	0.0	0.0
MALIAC13 ¹¹	ML Pc	6.84	12.59	15.82	90.0	94.0	90.0	-0.3	0.7	-0.1	0.0	0.5	0.0
MALNAC02 ¹²	MO β-form	7.77	8.08	12.19	77.7	77.7	70.0	-2.7	0.2	0.3	0.2	0.1	0.1
MALNAC10 ¹³	MO ε-form	13.15	6.91	25.65	90.0	97.7	90.0	-0.4	-0.9	-2.5	0.0	-0.1	0.0
OXLAC06 ¹⁴	OX α-form	25.44	4.91	9.76	90.0	96.3	90.0	-0.6	-1.8	-4.2	0.0	3.7	0.0
OXLAC11 ¹⁰	OX β-form	12.97	4.69	9.91	90.0	95.3	90.0	0.5	-2.3	0.6	0.0	-2.0	0.0
EXUQUJ ¹⁵	CA:GL 1:1 FII	7.41	10.15	7.54	90.0	124.6	90.0	-0.8	0.6	-0.1	0.0	0.2	0.0
EXUQUJ01 ¹⁵	CA:GL 1:1 FI	3.74	7.42	8.53	90.0	102.0	90.0	1.2	-0.8	-0.7	0.0	-0.2	0.0
GANYEA ¹⁶	CA:ML 1:1 FI	5.18	5.27	8.32	70.9	77.5	82.9	0.5	-1.4	-1.1	-0.8	1.8	-2.6
GANYEA01 ¹⁷	CA:ML 1:1 FII	4.75	34.37	7.81	90.0	98.4	90.0	-0.7	0.5	2.1	0.0	0.1	0.0
GANYIE01 ¹⁷	CA:ML 2:1	5.19	5.28	8.27	108.0	97.9	97.1	0.7	-0.9	1.2	0.0	-3.5	1.9
GANYAW ¹⁶	CA:MO 2:1	44.05	14.85	6.88	90.0	106.3	90.0	2.3	-1.5	-1.1	0.0	6.8	0.0
GANXUP ¹⁶	CA:OX 2:1	6.58	6.09	7.55	90.0	90.0	90.0	0.3	-0.1	-4.0	0.0	0.0	0.0

[a] Positive values indicate that the optimized cell is larger than the experimental unit cell.

Any change in unit cell parameters above 4% is unusual. The largest deviations are for CA:MO 2:1 which shows a 6.8% change in the angle of the unit cell, and OX α -form and CA:OX 2:1, which show deviations of 4% or more in one of the unit cell parameters.

Table S3: Lattice energies of the most stable polymorphs.

Molecule	Most stable polymorph energy Kcal/mol/molecule	Most stable polymorph
CA	-3653.752	Caffeine
GL	-2413.325	Glutaric acid β -form
ML	-1831.492	Maleic acid P2 ₁ /c
MO	-1639.372	Malonic β' -form
OX	-1245.356	Oxalic acid β -form

Table S4: Stabilities of the cocrystals[a]

Cocrystal	Energy of Coformers	Energy of Cocrystal	Stability of Cocrystal
CA:OX 2:1	-8552.9	-8562.2	-9.3
CA:MO 2:1	-8946.9	-8950.4	-3.5
CA:GL 1:1 FII	-6067.1	-6068.4	-1.3
CA:GL 1:1 FI	-6067.1	-6067.5	-0.4
CA:ML 1:1	-5485.2	-5486.4	-1.2
CA:ML 2:1	-9139.0	-9139.1	-0.1

[a] Energies are in kcal/mol of formula unit. The cocrystal is stable when the energy is negative.

14) pH measurements:

For each sample, the pH was determined at point zero (pH₀) and after 24 hours (pH₂₄). Slight variations were observed for pH values between the saturated solutions of the cocrystals, ranging between 1.0 and 2.5, which means that pH had no significant effect on S measurements (Table S5).

Table S5. pH levels at time 0, pH₀, and after 24 h, pH₂₄, for each cocrystal and relevant pure components:

Component	pH ₀	pH ₂₄	Cocrystal	pH ₀	pH ₂₄
CA	5.5	2.6	CA:OX 2:1	1.6	1.8
OX	1.3	1.2	CA:MO 2:1	1.9	1.5
MO	1.3	0.5	CA:GL 1:1 FII	2.1	2.3
GL	1.4	1.3	CA:GL 1:1 FI	-	-
ML	1.2	1.1	CA:ML 1:1	1.6	1.5
			CA:ML 2:1	-	-

15) Gibbs free energy change results:

The change in Gibbs free energy for coformer replacement reactions (ΔG_{Re}°) was calculated from measurements of the solubility products (K_{sp}), and equilibrium solubilities (S) in water for CA cocrystals and their pure components, respectively.

The changes in internal energy (ΔE) calculated by the DFT-D method in addition to ΔG_{Re}° values calculated from solubility data for coformer replacement reactions are listed in Table S6.

Table S6. Energy changes (kcal/mol) for coformer replacement reactions and cocrystal integrity observations whether replacement (Rep) is taking place (\checkmark) or not (X) under slurry processing.

Starting Cocrystal	SRD	Result	ΔE	ΔG_{Ex}°	Rep
CA:OX ^[b]	MO	CA:MO	5.79	7.50	X
CA:GL FII ^[c]			-0.82	-2.56	\checkmark
CA:GL FI ^[c]			-2.65	-*	\checkmark
CA:ML 1:1 ^[c]			-1.12	-1.03	\checkmark
CA:ML 2:1 ^[b]			-3.38	-*	\checkmark
CA:OX ^[d]	GL	CA:GL FII	7.96	11.44	X
CA:MO ^[d]			2.17	3.95	X
CA:GL FI ^[a]			-0.91	-*	\checkmark
CA:ML 1:1 ^[a]			-0.15	0.76	\checkmark
CA:ML 2:1 ^[d]			-1.21	-*	\checkmark
CA:OX ^[d]	GL	CA:GL FI	8.88	-*	X
CA:MO ^[d]			3.08	-*	X
CA:GL FII ^[a]			0.91	-*	X
CA:ML 1:1 ^[a]			0.76	-*	N/A
CA:ML 2:1 ^[d]			-0.30	-*	N/A
CA:OX ^[b]	ML	CA:ML 2:1	9.18	-*	X
CA:MO ^[c]			3.38	-*	X
CA:GL FII ^[c]			2.56	-*	X
CA:GL FI ^[c]			0.74	-*	X
CA:ML 1:1 ^[b]			2.27	-*	X

[a]: Reaction type 1 ($XY + Z \rightleftharpoons XZ + Y$), [b]: Type 2 ($X_2Y + Z \rightleftharpoons X_2Z + Y$), [c]: Type 3 ($2XY + Z \rightleftharpoons X_2Z + 2Y$), [d]: Type 4 ($X_2Y + Z \rightleftharpoons XZ + Y + X$), *: results could not be obtained due to experimental difficulties.

Supporting References:

- (1) Toda, F.; Trask, A.; Jones, W. In *Organic Solid State Reactions*; Springer Berlin Heidelberg, **2005**, 41–70.
- (2) Vangala, V. R.; Chow, P. S.; Tan, R. B. H. *Cryst. Growth Des.* **2012**, *12*, 5925–5938.
- (3) GRACE (the Generation, Ranking, and Characterization Engine) software package is a product of Avant-garde Materials Simulation. St-Germain-en-Laye, F. St-Germain-en-Laye, France 2015, p <http://www.avmatsim.eu>.
- (4) Kresse, G.; Joubert, D. *Phys. Rev. B* **1999**, *59*, 1758–1775.
- (5) Neumann, M. A.; Marc-Antoine Perrin. *J. Phys. Chem. B* **2005**, *109*, 15531–15541.
- (6) Schartman, R. R. *Int. J. Pharm.* **2009**, *365* (1-2), 77–80.
- (7) Enright, G. D.; Terskikh, V. V.; Brouwer, D. H.; Ripmeester, J. A. *Cryst. Growth Des.* **2007**, *7*, 1406–1410.
- (8) Lehmann, C. W.; Stowasser, F. *Chemistry* **2007**, *13*, 2908–2911.
- (9) Espeau, P.; Négrier, P.; Corvis, Y. *Cryst. Growth Des.* **2013**, *13*, 723–730.
- (10) Bhattacharya, S.; Saraswatula, V. G.; Saha, B. K. *Cryst. Growth Des.* **2013**, *13*, 3651–3656.
- (11) Day, G. M.; Trask, A. V.; Motherwell, W. D. S.; Jones, W. *Chem. Commun.* **2006**, *1*, 54–56.
- (12) Jagannathan, N. R.; Rajan, S. S.; Subramanian, E. *J. Chem. Crystallogr.* **1994**, *24*, 75–78.
- (13) Reddy, J. P.; Delori, A.; Foxman, B. M. *J. Mol. Struct.* **2013**, *1041*, 122–126.
- (14) Thalladi, V. R.; Nüsse, M.; Boese, R. *J. Am. Chem. Soc.* **2000**, *122*, 9227–9236.
- (15) Trask, A. V.; Motherwell, W. D. S.; Jones, W. *Chem. Commun.* **2004**, *7*, 890–891.
- (16) Trask, A. V.; Motherwell, W. D. S.; Jones, W. *Cryst. Growth Des.* **2005**, *5*, 1013–1021.
- (17) Leyssens, T.; Springuel, G.; Montis, R.; Candoni, N.; Veessler, S. *Cryst. Growth Des.* **2012**, *12*, 1520–1530.